Thermo-Mechanical Model for Wheel Rail Contact using Coupled Point Contact Elements

***J. Neuhaus[1] and W. Sextro[1]**

[1]Chair of Mechatronics and Dynamics, University of Paderborn, Pohlweg 47-49, 33098 Paderborn, Germany

*Corresponding author: jan.neuhaus@upb.de

Abstract

A model to calculate the locally resolved tangential contact forces of the wheel rail contact with respect to contact kinematics, material and surface properties as well as temperature is introduced.
The elasticity of wheel and rail is modeled as an elastic layer consisting of point contact elements connected by springs to each other and to the wheel. Each element has two degrees of freedom in tangential directions. The resulting total stiffness matrix is reduced to calculate only the position of the elements in contact. Friction forces as well as contact stiffnesses are incorporated by a nonlinear force-displacement characteristic, which originates from a detailed contact model. The contact elements are transported through the contact zone in discrete time steps. After each time step an equilibrium is calculated. For all elements, their temperature and its influence on local friction are regarded by calculating friction power and temperature each time step.

Keywords: Rolling Contact, Discrete Elements, Contact Stiffness, Temperature

Introduction

To calculate the tangential contact forces in wheel rail systems for e.g. vehicle dynamics, a profound knowledge of the creep force characteristic is necessary. To achieve this, the creep dependent distribution of tangential forces inside the contact zone is necessary. Especially at higher slip the temperature in the contact zone becomes high enough to effect significantly on the tangential forces.
Many approaches have been made to calculate the tangential force distribution. Kalker [Kalker (1967); Kalker (1990)] developed the program CONTACT to calculate contact forces. This program assumes Hertzian contact and halfspace assumption to calculate the traction forces. Due to halfspace assumption the computation times are very high. Approaches have been made to reduce computation time compared to CONTACT [Kalker (1982); Polach (2000)], however these do not include temperature effects.
In [Sextro (2007)] a numerical model for the wheel rail contact is developed. The contact zone is discretized and each partial area is described by a point contact element. A single point contact element includes differential contact stiffness as well as a nonlinear partial friction force. By applying deformations on the point contact elements, which are deduced from the kinematics of wheel and rail, the tangential force distribution in the contact zone can be calculated. Also temperature and its influence on the friction coefficient are regarded in this approach.
In [Tomberger et. al (2011)] a model for the wheel rail contact comprising roughness interfacial fluids and temperature is shown. The tangential contact is discretized using independent contact stiffnesses as suggested in [Sextro (2007)]. The modeling method is based on FASTSIM, but allows varying coefficients of friction. In a micro contact model the effects of interfacial fluids and temperature on the friction coefficient are calculated with respect to roughness, contact kinematics and material properties.

Also, the Finite Element Method has been used to calculate forces in the rolling contact. Nackenhorst [Nackenhorst (2004)] used an arbitrarian lagrangian eulerian formulation for calculating contact forces using the Finite Element Method for stationary rolling contact. By splitting the motion into rigid body motion and elastic deformation and solving the transportation problem of wheel and rail elements through the contact zone similar to transport problems in fluid dynamics. The contact forces can be calculated by this method retaining a fine mesh in the contact zone and a large mesh outside of it.
In [Wen et al. 2011] and [Zhao and Li 2011] the tangential forces in wheel rail contact where calculated using Finite Elements models. However, temperature effects were not taken into account and the computation time for these models is very high.
The model presented here is based on the approach by Sextro [Sextro (2007)]. Instead of using independent point contact elements, the elasticity of wheel and rail is modeled by an elastic layer, to better model the elastic deformation inside the contact zone. The algorithm used in this model computes the tangential contact forces at stationary rolling by computing equilibrium of the forces caused by the elastic layer and the tangential contact forces. Additionally, the influence of roughness and temperature can be investigated with this model.

Contact Kinematics

The kinematics of a rigid wheel rolling over a rigid rail under slip angle α and angular velocity ω are depicted in Fig. 1.

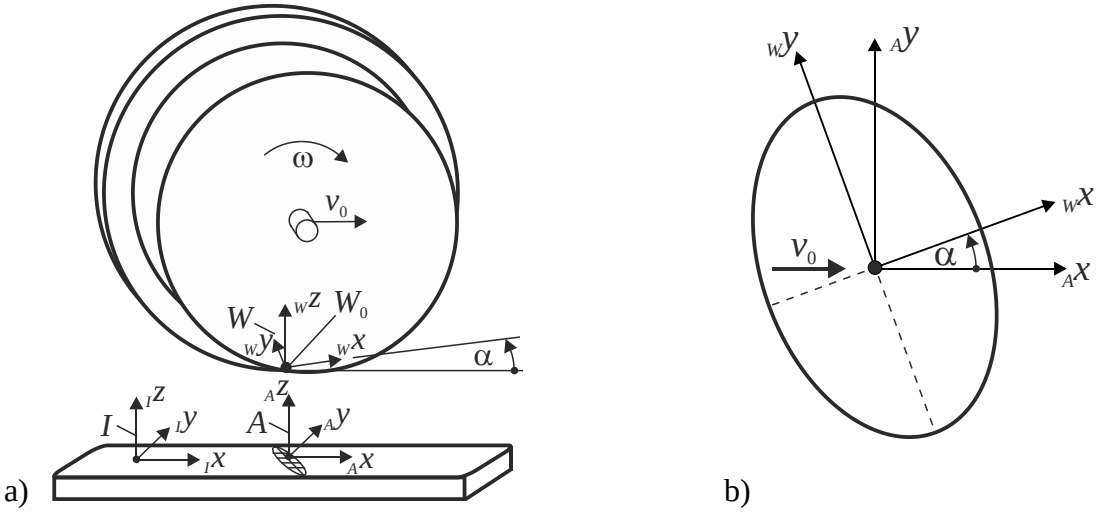

a) b)

Figure 1, Wheel and Rail Schematic

The wheel shown in Fig. 1 a) is moving relative to the inertia frame *I* in ${}_I x$-direction with constant velocity v_0. The contact patch shown in Fig. 1b) is described by the reference system *A*, which is also moving with the wheel center in ${}_I x$-direction with velocity v_0. A point on the wheel's surface in contact is described by the wheel fixed coordinate system *W*, which is rotated relative to the inertia system around the ${}_I z$-axis by a constant angle α. The angular velocity of the wheel is defined relative to the wheel fixed coordinate system *W* with

$$ {}^{IW}_{W}\underline{\omega} = [0 \quad \omega \quad 0]^T . \tag{1}$$

The inertia system *I* is fixed on the rail. The tangential velocity of the point W_0 on the wheel in the contact is dependent on the angular velocity and the slip angle α and can be calculated by

$$ {}^{I}_{I}\underline{v}_{W_0} = \begin{bmatrix} v_0 - \omega R\cos\alpha & -\omega R\sin\alpha & 0 \end{bmatrix}^T . \tag{2} $$

The longitudinal slippage *s* can be calculated with

$$ s = \frac{v_0 - \omega R}{v_0} . \tag{3} $$

In the following, all vectors will be given in coordinates of the *W*-system, unless noted otherwise.

Contact Model

Modelling approach

The creep force characteristic of wheel and rail is highly dependent on the elastic deformations inside the contact area. The elasticity of wheel and rail is modeled as an elastic layer consisting of discrete elements having an elasticity equivalent to the combined elasticity of wheel and rail. A detail of the elastic layer is shown in Fig. 2 a). The layer consists of coupled massless point contacts *P* connected by springs with spring stiffnesses $\Delta c_{k,x}$ and $\Delta c_{k,y}$ in tangential direction to each other. The layer is also coupled by springs with stiffnesses Δc_x and Δc_y to the rigid wheel in ${}_W x$- and ${}_W y$-direction respectively.

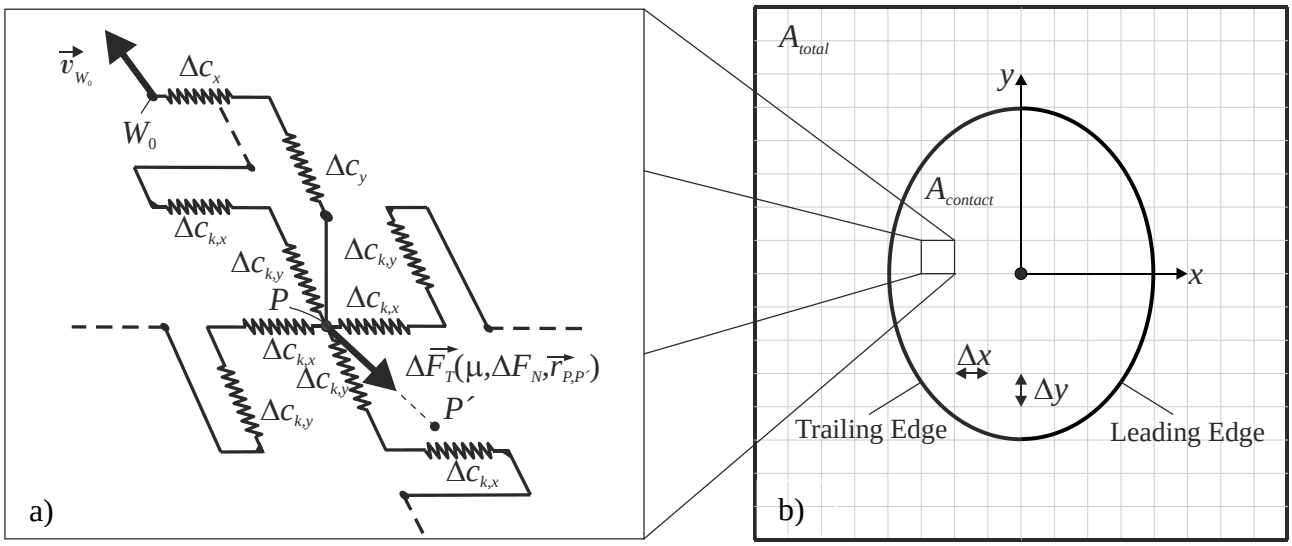

Figure 2, Elastic Layer and Contact Area

If the point *P* is inside the contact area, a nonlinear tangential force $\vec{F}_T(\mu,\Delta F_N,\vec{r}_{P,P'})$ applies, which is described in detail later in this paper. *P´* is a point which is fixed on the rail, so $\vec{r}_{P,P'}$ is the sliding distance of *P*, which is also the displacement of *P* relative to the rail. The tangential forces cause deformations which influence the neighborhood around the contact area and vice versa. Therefore, not only the contact area but also the surrounding area A_{total} is modeled with the elastic layer. The size of the total area A_{total} is not as large as the total wheel's surface but large enough, that deformations at the edge of the total area are diminishing small compared to the deformations inside the contact area. The discretised elliptical contact area with the surrounding total area is shown in

Fig. 2 b). The total area is discretised in rectangular partial areas with the dimensions Δx and Δy. The position of the contact area border in drive direction is referred in the following as leading edge. The elastic layer can be described by a set of linear coupled equations. The relation between force and displacement with respect to the wheel coordinate system *W* is:

$$\begin{bmatrix} \underline{F}_T \\ \underline{0} \end{bmatrix} = \begin{bmatrix} \underline{C}_{ii} & \underline{C}_{io} \\ \underline{C}_{oi} & \underline{C}_{oo} \end{bmatrix} \begin{bmatrix} \underline{r}_{P,i} \\ \underline{r}_{P,o} \end{bmatrix}. \tag{4}$$

The force and displacement vectors in this equation have been sorted for point elements inside the contact area with index *i* and outside the contact area with index *o*. The displacement vectors can be written as

$$\underline{r}_{P,i} = \begin{bmatrix} r_{P1,x,i} & r_{P1,y,i} & r_{P2,x,i} & r_{P2,y,i} & \cdots \end{bmatrix}^T \text{ and } \underline{r}_{P,o} = \begin{bmatrix} r_{P1,x,o} & r_{P1,y,o} & r_{P2,x,o} & r_{P2,y,o} & \cdots \end{bmatrix}^T. \tag{5}$$

$r_{P,x}$ and $r_{P,y}$ are the displacements of the point *P* in *x*- and *y*-direction respectively.
In order to reduce computational effort, the equation system is reduced to calculate only the forces and displacements inside the contact area. The displacements of the points outside the contact area can be calculated by the second row of the block matrix equation Eq. (4):

$$\underline{r}_{P,o} = -\underline{C}_{oi} \underline{C}_{oo}^{-1} \underline{r}_{P,i}. \tag{6}$$

Inserting Eq. (6) in the first row of Eq. (4) leads to

$$\underline{F}_T = \underbrace{\left(\underline{C}_{ii} - \underline{C}_{oi} \underline{C}_{oo}^{-1} \right)}_{\underline{C}_{red}} \underline{r}_{P,i}. \tag{7}$$

So, the relation between tangential forces and tangential displacements in contact can be described by a linear equation system with reduced stiffness matrix $\underline{C}_{red}$.

Nonlinear Tangential Force

The elasticity of wheel and rail is modeled as described above. Due to the roughness of surfaces in contact a normal pressure dependent contact stiffness develops. Furthermore, the tangential force for sticking and sliding conditions has to be applied at point *P*. This is regarded by a nonlinear force displacement characteristic, derived from a detailed micro contact model [Neuhaus and Sextro (2013)]. Using this model, the tangential force including the transition from sticking to sliding can be computed using measured rough surfaces for different nominal normal pressures. The curves achieved from this simulation can be approximated by adequate analytical functions for efficient use in the rolling contact model. Figure 3 shows a result using this micro contact model. The development of the normalized force while moving two surfaces tangentially against each other is shown. The slope at normalized tangential displacement of zero can be interpreted as contact stiffness while sticking. Full sliding is indicated by a gradient of zero of the force displacement curve.
Pure sticking only exists when no tangential force applies; afterwards the curve rises nonlinear and continuously goes over to sliding. This curve can be approximated well by an exponential function. In case of monotone relative movement in constant direction this force displacement characteristic can be used to model sticking and sliding, because the displacement vector always points in the same direction as the velocity vector.

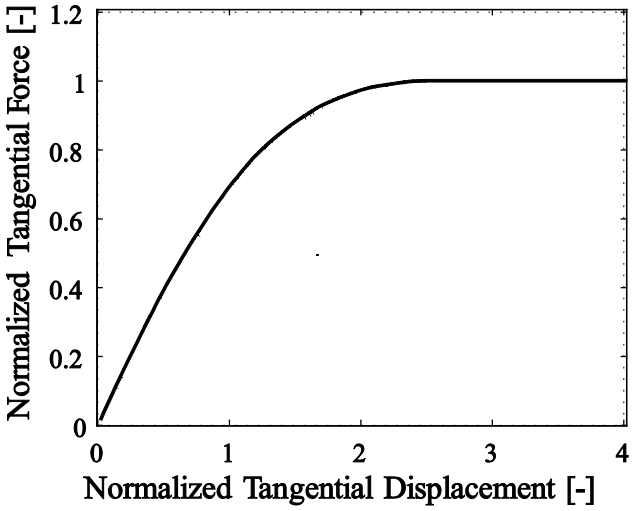

Figure 3, Tangential Force

The tangential force on a single point contact P is dependent on the sliding distance of P and thus of the magnitude of $\vec{r}_{P,P'}$ and its direction. As mentioned above, it can be calculated by an exponential law which approximates the force displacement characteristic seen in Fig. 3 with

$$\Delta \underline{F}_T = \mu \Delta F_N \left(1 - e^{-k_c \left|\underline{r}_{P,P'}\right|}\right) \frac{{}_W\underline{r}_{P,P'}}{\left|\underline{r}_{P,P'}\right|} \tag{8}$$

where $\frac{{}_W\underline{r}_{P,P'}}{\left|\underline{r}_{P,P'}\right|}$ is the unit vector pointing opposite to the sliding direction.

The corresponding differential normal force is calculated according to a given normal pressure distribution. The normal pressure distribution can be achieved for example by using the Hertzian Theory, Finite element calculations or measurement results.

Simulation procedure

The rolling contact is simulated by transporting the elastic layer as described above through the contact area in discrete time steps Δt. The transporting velocity relative to the contact coordinate system A given in coordinates of the wheel system W is

$${}^A\underline{v}_t = \begin{bmatrix} -\omega R & 0 & 0 \end{bmatrix}^T . \tag{9}$$

In order to maintain a constant grid, the value of Δt is chosen in a way that an element is transported the distance Δx in one time step. So, the position $\vec{r}_{W_0}$ of point W_0 is equal to the position of its successor in negative x -direction after one time step if

$$\Delta t = \frac{\Delta x}{\omega R} . \tag{10}$$

Because P' is fixed to the rail a relative differential displacement $\Delta\vec{r}_{W_0,P}$ between W_0 and P' applies after each time step Δt. It is the displacement between a point on the rigid wheel and a point on the

rigid rail after one time step and can be expressed relative to the contact coordinate system *A* assuming small angles α by

$$\Delta_A \underline{r}_{W_0,P'} = \begin{bmatrix} v_0 - \omega R & -\omega R\alpha & 0 \end{bmatrix}^T \Delta t \tag{11}$$

or with respect to the wheel coordinate system *W* by

$$\Delta \underline{r}_{W_0,P'} = \begin{bmatrix} v_0 - \omega R & -v_0\alpha & 0 \end{bmatrix}^T \Delta t\,. \tag{12}$$

This differential relative displacement $\Delta\vec{r}_{W_0,P}$ is added to the position vector of P', $\vec{r}_{P'}$, after each time step.
For new elements entering the contact area at the leading edge, the position vector $\vec{r}_{P'}$ is set to their position vector $\vec{r}_P$ immediately before entering the contact, such that $\vec{r}_{P,P'} = \vec{0}$. After applying the relative differential deformation for one time step, an equilibrium between the nonlinear tangential force defined in Eq. 8 and the forces from the elastic layer is found according to Eq. 7 by

$$\underline{C}_{red\,W}\,\underline{r}_{P,i} - {}_W\underline{F}_T = \underline{0} \tag{13}$$

with

$$\underline{F}_R = \begin{bmatrix} \Delta F_{R,1}^T & \Delta F_{R,1}^T & \cdots & \Delta F_{R,nk}^T \end{bmatrix}^T \tag{14}$$

where n_k is the number of elements in contact.
The equilibrium for Eq. 13 is found by using the Newton Raphson method. Firstly, the gradient of the tangential force $\frac{\partial \underline{F}_T}{\partial \underline{r}_{P,i}}$ has to be calculated, which can be done due to the analytical description of the force displacement characteristic. Secondly, the Jacobian $\underline{J}$ is calculated by adding the force gradient of the nonlinear tangential force to the constant gradient emerging from the reduced stiffness matrix shown in Eq. 15:

$$\underline{J} = \underline{C}_{red} + \frac{\partial \underline{F}_T}{\partial \underline{r}_{P,i}^T} \tag{15}$$

Using the Jacobian from Eq. 15, a differential displacement can be calculated and added to the displacement vector ${}_W\underline{r}_{P,i}$ iteratively until the equilibrium condition of Eq. 13 is fulfilled within an relative error ε_{rel}.

$$\left| \underline{C}_{red}\,\underline{r}_{P,i} - \underline{F}_T \right| < \varepsilon_{rel}\mu F_N \tag{16}$$

After finding the equilibrium for a defined tolerable error ε a new time step is calculated until a steady state is reached in the contact area. This is usually the case, when an element entering the contact area at simulation start has crossed and left it at the trailing edge.

Temperature Model

Caused by high contact pressure in the wheel rail contact and consequently high friction power, the temperature in the contact zone plays an important role to describe the friction behavior correctly. Therefore, this effect is considered in this model. The model used here is adapted from the temperature model described in [Sextro (2006)]. The friction power for a single element can be calculated by

$$\Delta P_R = \Delta \left| \underline{F}_R \right\| \underline{v}_P \left| \right. . \tag{17}$$

The heat source q_H can be calculated relating the friction power to a partial area

$$q_H = \frac{\Delta P_R}{\Delta A}, \quad \Delta A = \Delta x \Delta y . \tag{18}$$

Assuming a high Peclet number, Knothe and Liebelt [Knothe and Liebelt (1990)] showed, that the three dimensional heat transfer problem can be reduced to a two dimensional problem for a strip in *x*-direction using the approximated heat transfer equation

$$v_0 \frac{\partial T}{\partial x} = \kappa \frac{\partial^2 T}{\partial z^2} \tag{19}$$

with the thermal diffusivity defined as

$$\kappa_W = \frac{\lambda_W}{\rho_W c_W}, \tag{20}$$

where λ_W denotes the heat conductivity, ρ_W the density and c_W the specific heat capacity of the wheel [Sextro (2006)]. Assuming a constant heat source, the temperature distribution in *x*-direction, the temperature at time step *j* can then be calculated using the temperature at the element at time step *j*-1 by

$$T_j^2 = T_{j-1}^2 + \Delta T^2 . \tag{21}$$

The temperature difference ΔT is computed as

$$\Delta T = \frac{2}{\sqrt{\pi}} \sqrt{\frac{\kappa_W}{v_0}} \frac{\alpha_W q_H}{\lambda_W} \sqrt{\Delta x} \tag{22}$$

with α_W as the heat partitioning factor between wheel and rail. For low slippage the factor can be assumed to be 0.5, this means heat is equally distributed between wheel and rail. Otherwise it can be calculated from the velocities of the contact relative to wheel and rail. For details see [Sextro (2006)]. Using this approach, the maximum temperature occurs at the trailing edge due to the assumption of constant heat distribution, but in fact the temperature reaches its maximum shortly before the trailing edge due to the not-constant heat distribution. However this procedure can be used to regard temperature influence because the temperature distribution in the main contact area where most of the forces are transmitted is approximated well.

In principle, due to the mutual interaction between friction power, temperature and friction coefficient, an iterative loop inside the computation of a single time step is necessary. This can be skipped, because the temperature and thus the temperature dependent friction coefficient converge within the time step simulation. The temperature dependent friction coefficient at time step *j+1* is assumed to be approximate equal to the temperature dependent friction coefficient at time step *j*. Using this procedure usually a steady state is reached after an element is transported through the complete contact area.

Thus the temperature dependent friction coefficient of time step *j+1* is calculated using a linear relationship between the friction coefficient μ_0 and temperature at time step *j*

$$\mu_{j+1} \approx \mu_j = \mu_0 \left(1 - \frac{T_j}{T_E} \right) \tag{23}$$

where T_E defines the slope of the temperature dependency.

Results

The equations above have been implemented in MATLAB to model the rolling contact. The results shown in the following are normalized and therefore have qualitative character. This will be done in future by comparing the deformations of the elastic layer with the deformation computed by a Finite Element model and adapting the spring stiffnesses to minimize the deformation difference. Nonetheless the results show that the effects in rolling contact can be modeled plausibly. For the simulations, the normal pressure has been calculated according to Hertzian theory. The normalized normal pressure distribution

$$p^* = \frac{p_N}{p_{N_{\max}}} \tag{24}$$

is shown in Fig. 4. The *x** and *y** coordinates have been normalized to the ellipsis half axes.

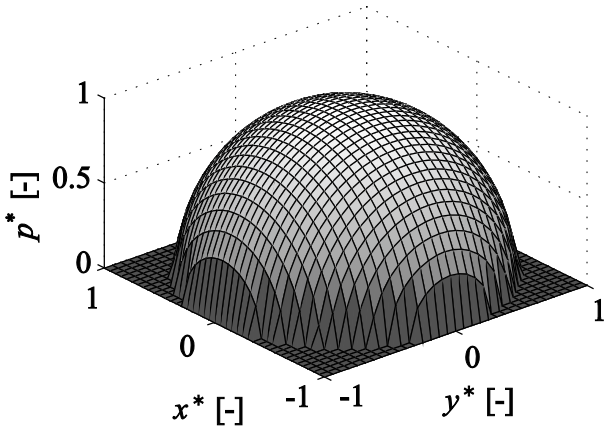

Figure 4 Normal Pressure Distribution

Fig. 5 shows the tangential force in *x*-direction normalized to the maximal transmittable tangential force with

$$\Delta F_T^* = \frac{\Delta F_T}{\mu_0 p_{N_{\max}} \Delta A}. \tag{25}$$

The simulation has been performed at pure longitudinal slip s of 0.008. The leading edge is seen front right. A zone with sticking friction, behind the leading edge can be identified with a linear rising tangential force towards the trailing edge shown in Fig. 5a) where almost no sliding velocity exists, as shown in Fig. 5b). Also a region with sliding friction can be seen towards the trailing edge. Here, the shape of the tangential force distribution equals the normal pressure distribution and the sliding velocities rise towards the trailing edge. The step in the shown tangential force at the leading edge and at the transition from sticking to sliding is caused by the coupling stiffnesses. Qualitatively the shape of the tangential force distribution matches well with Kalker's theory and Finite element calculations.

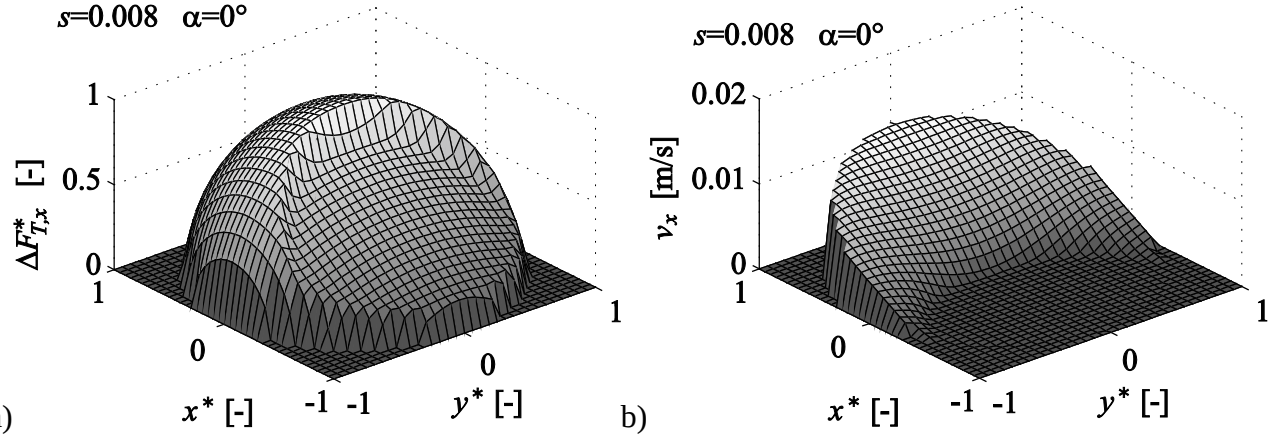

a) b)

Figure 5 Tangential Force Distribution and Sliding Velocity

In Fig. 6 the tangential forces in x- and y-direction for a longitudinal slip s of 0.008 and slip angle α of 0.5 degrees are shown.

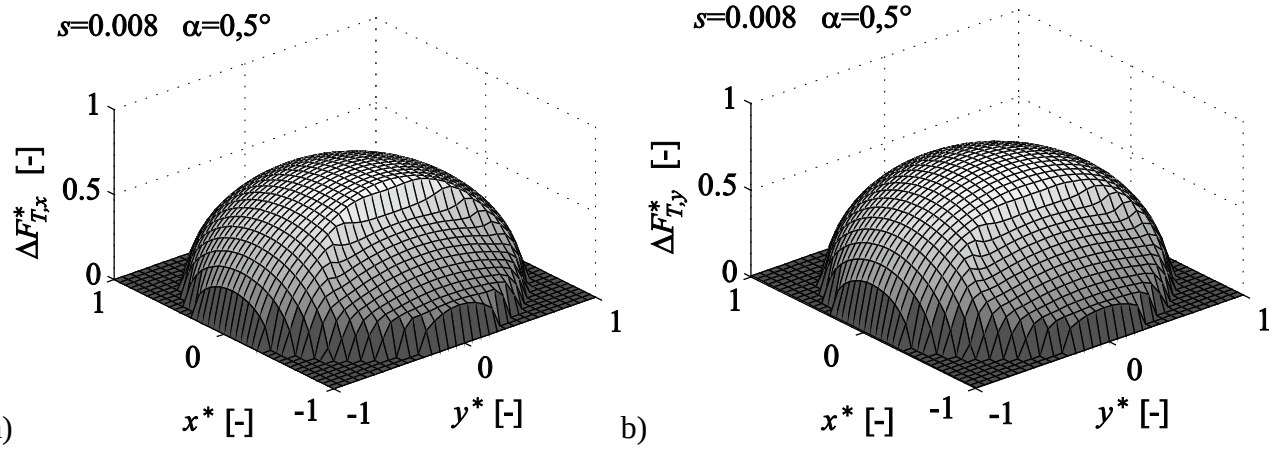

a) b)

Figure 6 Tangential Force Distribution in x- and y-Direction

Compared to pure longitudinal slip, the total tangential force in x-direction is significantly lower, because lateral forces in y-direction occur at this slip angle, which is shown in Fig. 6b). Also the area with sliding friction is larger compared to the case with pure longitudinal slip in Fig. 5.

The friction power for each partial area ΔP_R and the temperature difference ΔT relative to the surrounding are shown in Fig. 7 a) and b) respectively for combined slip. The friction power reaches its maximum just before the trailing edge due to the tangential force and sliding velocity

distribution. In the sticking region, the friction power is zero. As described at the temperature model, temperature reaches its maximum at the trailing edge.

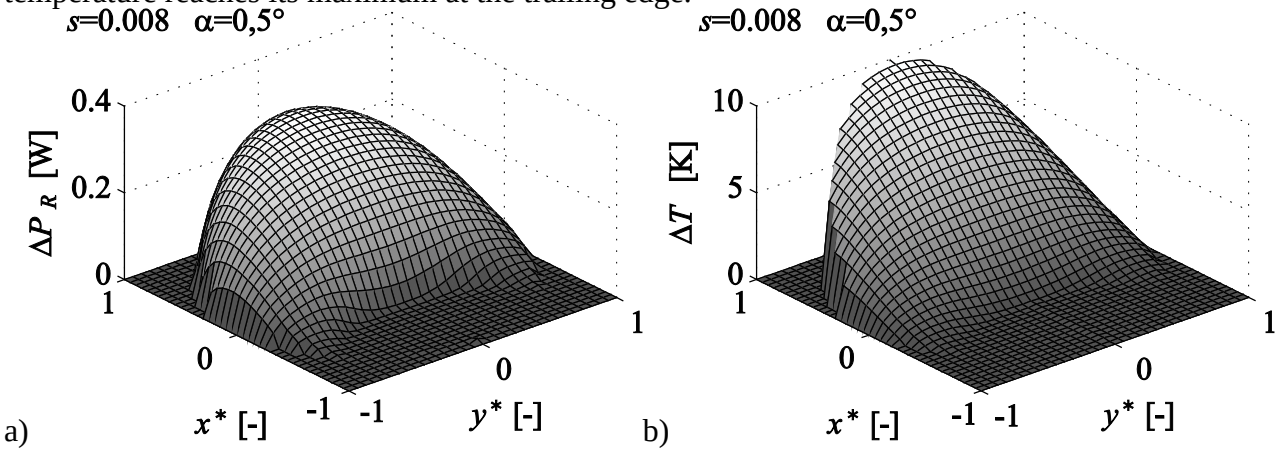

Figure 7 Friction Power and Temperature

The computing time for one simulation was 19 seconds on an Intel i7 processor using 2 of 4 cores. This is quite low compared to computationally intensive Finite Element models.

Conclusions

A model for calculating the tangential forces in the wheel rail contact comprising contact stiffness and temperature has been developed. The model is based on the rolling contact model of Sextro [Sextro (2006)]; however the point contacts are coupled with each other to model an elastic layer which represents the elasticity of wheel and rail. Also, a nonlinear tangential force is applied to the coupled massless points, to model contact stiffness as well as sticking and sliding friction. The set of equations for describing contact and surrounding area can be reduced to compute only forces and displacements inside the contact area which reduces computation time. The simulation is carried out in discrete time steps, in which the elastic layer is moved through the contact area and an equilibrium is calculated after each time step. Temperature and its influence on the friction coefficient are calculated as in the model of Sextro [Sextro (2006)] assuming a high Peclet number and constant heat source distribution. This is a satisfying approximation for the exact solution of elliptical heat source distribution.

The simulation produces plausible results for tangential force distribution under pure longitudinal and combined slip. Friction power and temperature distribution match qualitatively well compared to other modeling methods.

References

Kalker, J. J. (1967). *On the rolling contact of two elastic bodies in the presence of dry friction* (Doctoral dissertation, Delft University)

Kalker, J. J. (1990). *Three-dimensional elastic bodies in rolling contact* (Vol. 2). Springer.

Kalker, J. J. (1982). A fast algorithm for the simplified theory of rolling contact. *Vehicle System Dynamics*, *11*(1), 1-13.

Polach, O. (2000). A fast wheel-rail forces calculation computer code. *Vehicle System Dynamics*, *33*, 728-739.

Sextro, W. (2007). *Dynamical contact problems with friction: models, methods, experiments and applications*. Springer.

Tomberger, C., Dietmaier, P., Sextro, W., & Six, K. (2011). Friction in wheel–rail contact: a model comprising interfacial fluids, surface roughness and temperature. *Wear*, *271*(1), 2-12.

Nackenhorst, U. (2004). The ALE-formulation of bodies in rolling contact: theoretical foundations and finite element approach. *Computer Methods in Applied Mechanics and Engineering*, *193*(39), 4299-4322.

Wen, Z., Wu, L., Li, W., Jin, X., & Zhu, M. (2011). Three-dimensional elastic–plastic stress analysis of wheel–rail rolling contact. *Wear*, *271*(1), 426-436.

Zhao, X., & Li, Z. (2011). The solution of frictional wheel–rail rolling contact with a 3D transient finite element model: Validation and error analysis. *Wear*, *271*(1), 444-452.

Neuhaus, J.; Sextro, W. (2013): A Discrete 2D Model for Dynamical Contact of Rough Surfaces. *3rd International Conference on Computational Contact Mechanics 2013, 2013*

Knothe, K., & Liebelt, S. (1995). Determination of temperatures for sliding contact with applications for wheel-rail systems. *Wear*, *189*(1), 91-99.